PROCEEDINGS, 47th Workshop on Geothermal Reservoir Engineering
Stanford University, Stanford, California, February 7-9, 2022
SGP-TR-223

Machine Learning Enhanced Seismic Monitoring at 100 km and 10 m Scales

Chengping Chai[1], Monica Maceira[1] and EGS Collab Team[†]

[1]Oak Ridge National Laboratory, Oak Ridge, TN 37930, USA

Email: chaic@ornl.gov (Chai), maceiram@ornl.gov (Maceira)

Keywords: machine learning, deep learning, seismic monitoring, geothermal energy, EGS Collab

ABSTRACT

Rapid and accurate monitoring of seismicity is crucial for both reservoir management and risk mitigation. It is important to monitor not only seismic events due to hydraulic fracturing but also naturally occurring background seismicity. Depending on the size of the reservoir, monitoring of background and induced seismicity usually deals with different spatial scales. Thanks to an expanded station coverage and continuous improvements on seismic sensors, a large amount of data has been collected for both natural and induced seismicity. Traditional seismic data processing techniques can provide rapid and automatic seismic event catalogs or more accurate results but at a higher time and labor cost. To obtain accurate seismicity catalogs rapidly and extract valuable information from large amounts of data effectively, we developed a machine learning enhanced seismic monitoring workflow that combines cutting-edge machine learning techniques and advanced seismic data processing algorithms. The workflow is suitable for the monitoring of both natural and induced seismicity at dramatically different spatial scales. To demonstrate this capability, we applied the workflow to the Oklahoma region as an example for 100 km scale sites and to the experiment 1 site of the EGS Collab project with a length scale of 10 m. Our workflow not only produces high-precision seismicity catalogs but also images the 3D subsurface structure with high resolution. We compare our results against those from traditional techniques.

1. INTRODUCTION

Seismic event catalogs and subsurface structure are not only crucial for selecting and/or evaluating geothermal and carbon storage sites but also essential for risk monitoring of existing sites. High-precision seismic event catalogs and high-resolution images of the subsurface are necessary for reliable decision-making related to reservoir management. Imaging the subsurface requires significant time and effort from experienced researchers. Existing seismic monitoring approaches can provide crude seismic locations quickly or high-resolution results after months or years of dedicated research. The current state of practice uses automatic algorithms to scan through continuous data, detect seismic events related signals, and measure seismic phase arrival times. These automatic algorithms are usually fast. But arrival times measured by the traditional approaches such as short-term-average/long-term-average (STA/LTA, Allen, 1978) are not accurate enough for locating seismic events precisely. As manually measured arrival times are the most reliable approach, human analysts usually refine the automatic arrival time measurements by visually looking through a large number of seismograms one by one. Picking these arrival times is very labor-intensive. This labor-intensive step is the bottleneck of high-precision seismic monitoring. High-precision seismic catalogs take months if not years to develop. Thanks to recent developments in machine learning techniques, many deep learning models are available for seismic arrival time picking (e.g., Mousavi et al., 2020; Ross et al., 2018; Zhou et al., 2019; L. Zhu et al., 2019; W. Zhu & Beroza, 2018). However, applications of these deep learning models at different spatial scales are limited. Our objective is to speed up these labor-intensive steps with machine learning (ML) techniques and integrate them with advanced geophysical imaging algorithms to form an artificial intelligence (AI) enhanced workflow for fast and high-precision seismic monitoring.

[†]J. Ajo-Franklin, T. Baumgartner, K. Beckers, D. Blankenship, A. Bonneville, L. Boyd, S. Brown, J.A. Burghardt, C. Chai, Y. Chen, B. Chi, K. Condon, P.J. Cook, D. Crandall, P.F. Dobson, T. Doe, C.A. Doughty, D. Elsworth, J. Feldman, Z. Feng, A. Foris, L.P. Frash, Z. Frone, P. Fu, K. Gao, A. Ghassemi, Y. Guglielmi, B. Haimson, A. Hawkins, J. Heise, C. Hopp, M. Horn, R.N. Horne, J. Horner, M. Hu, H. Huang, L. Huang, K.J. Im, M. Ingraham, E. Jafarov, R.S. Jayne, S.E. Johnson, T.C. Johnson, B. Johnston, K. Kim, D.K. King, T. Kneafsey, H. Knox, J. Knox, D. Kumar, M. Lee, K. Li, Z. Li, M. Maceira, P. Mackey, N. Makedonska, E. Mattson, M.W. McClure, J. McLennan, C. Medler, R.J. Mellors, E. Metcalfe, J. Moore, C.E. Morency, J.P. Morris, T. Myers, S. Nakagawa, G. Neupane, G. Newman, A. Nieto, C.M. Oldenburg, T. Paronish, R. Pawar, P. Petrov, B. Pietzyk, R. Podgorney, Y. Polsky, J. Pope, S. Porse, J.C. Primo, C. Reimers, B.Q. Roberts, M. Robertson, W. Roggenthen, J. Rutqvist, D. Rynders, M. Schoenball, P. Schwering, V. Sesetty, C.S. Sherman, A. Singh, M.M. Smith, H. Sone, E.L. Sonnenthal, F.A. Soom, P. Sprinkle, C.E. Strickland, J. Su, D. Templeton, J.N. Thomle, V.R. Tribaldos, C. Ulrich, N. Uzunlar, A. Vachaparampil, C.A. Valladao, W. Vandermeer, G. Vandine, D. Vardiman, V.R. Vermeul, J.L. Wagoner, H.F. Wang, J. Weers, N. Welch, J. White, M.D. White, P. Winterfeld, T. Wood, S. Workman, H. Wu, Y.S. Wu, E.C. Yildirim, Y. Zhang, Y.Q. Zhang, Q. Zhou, M.D. Zoback

We use two sites to demonstrate our seismic monitoring workflow and compare our results with existing techniques. One of them is the Experiment 1 site of the EGS Collab project that is located at the 4,850-ft level (around 1.5 km beneath the surface) of the Sanford Underground Research Facility (Lead, South Dakota). The Experiment 1 site has a spatial dimension of 10 meters (Figure 1a). Hundreds of microseismic events related to several hydraulic stimulations have been recorded at the site. Schoenball et al. (2020) produced a seismic catalog after intensive study. We will refer to it as the initial catalog hereafter. We compare our results against Schoenball et al. (2020) for the EGS Collab Experiment 1 site. The other site is the Oklahoma region which has a spatial dimension of 100 km (Figure 1b). Our results for the Oklahoma region are compared against the earthquake catalog from the United States Geological Survey (USGS) due to its wide availability.

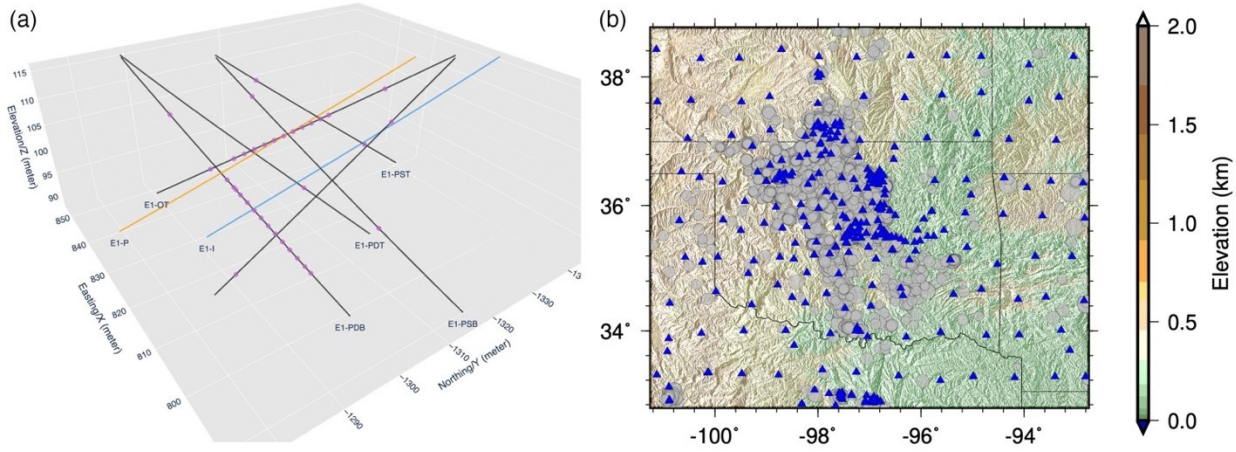

Figure 1: Two study areas at (a) 10 m scale and (b) 100 km scale. In panel a, lines represent boreholes. The blue line is the injection well. The yellow line is the production well. Black lines are monitoring wells. Purple dots represent seismic sensors. In panel b, gray circles represent seismic events. Blue triangles are seismic stations.

2. EGS COLLAB EXPERIMENT 1

The EGS Collab Experiment 1 site had one injection, one production, and six 60 m-long monitoring wells (see Figure 1a for the layout). Inside the monitoring wells, we deployed 24 single-component and 12 three-component seismic sensors. Several hydraulic stimulations were carried out in May 2018, June 2018, July 2018 and December 2018. We focus on the days that these hydraulic stimulations were conducted. Details about the stimulations can be found in Schoenball et al. (2020) and Fu et al. (2021). Chai et al. (2020) developed a transfer learned model for the site by fine-tuning a deep learning model called PhaseNet (W. Zhu & Beroza, 2018), which was designed for natural earthquakes and at a 100-km scale. Double-difference tomography (Zhang & Thurber, 2003, 2006) has been applied to manually measured arrival times (Chai, Maceira, et al., 2021). In this study, we integrate the transfer learned model and the double-difference tomography for continuous seismic data.

2.1 Data

Our data for the EGS Collab Experiment 1 site consist of 13 days of continuous seismic data (around 40 TB) recorded at the 35 seismic sensors (one sensor was defective) between May 2018 and December 2018, when hydraulic stimulations were carried out. The data was sampled at 100 kHz. Crosstalk from the electrical resistivity tomography sensors, electrical spikes from the recording system, and active seismic shots about every 0.8 s from the continuous active seismic source monitoring system contaminated the seismic signals. We followed the same procedures as Schoenball et al. (2020) to reduce these effects. Additional details about the experiment design and the monitoring system can be found in Schoenball et al. (2020).

2.2 Method

As shown in Figure 2, we applied the transfer learned model to continuous data to detect signals related to microseismic events and measure seismic phase arrival times. A modified version of Hypoinverse (Klein, 2002) was use to obtain an initial catalog of seismic events. We visually inspected the seismic events using interactive visualization tools similar to Chai et al. (2018) and found that a significant number of active source events were included in the initial catalog. We used the density-based spatial clustering of applications with noise (DBSCAN) and excluded most of the active source events. The initial catalog as well as the associated phase picks were used in the double-difference tomography package to further improve the seismic event locations. The resulting catalog will be referred to as the update catalog.

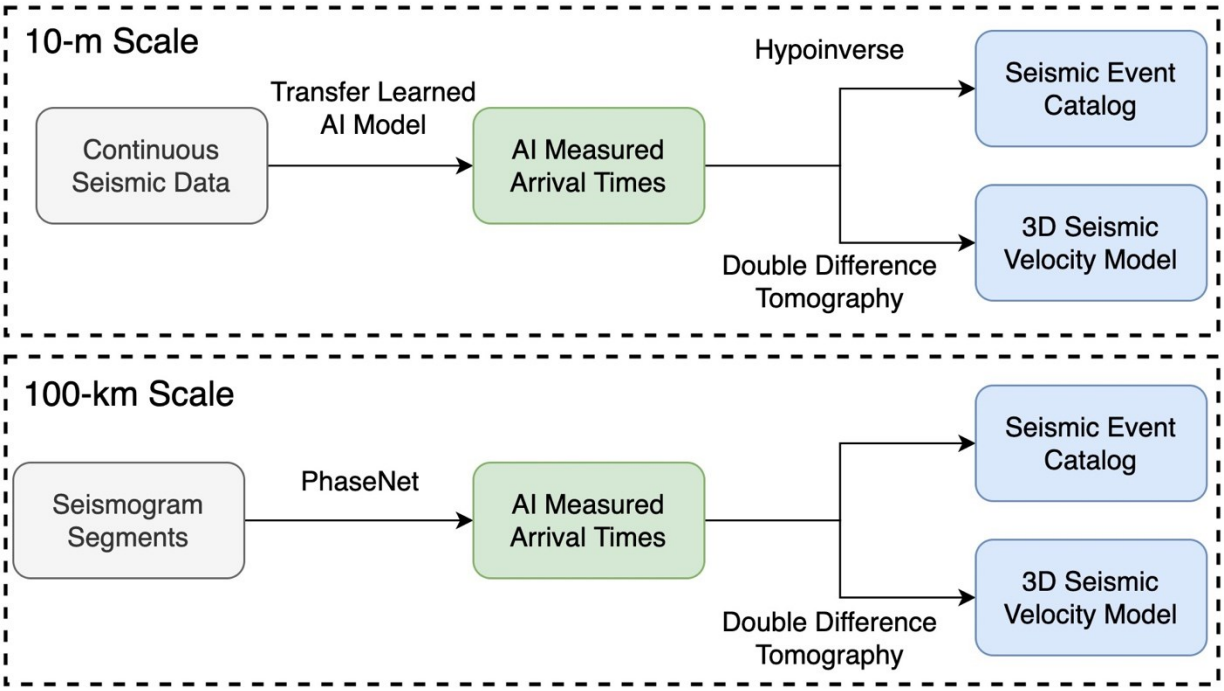

Figure 2: Flowcharts showing the major component of our AI-enhanced workflow for seismic monitoring (top) at 10-m scale and (bottom) at 100-km scale. The transfer learned model is obtained from Chai et al. (2020). Hypoinverse was designed by Klein (2002). Double-difference tomography was developed by Zhang & Thurber (2003). PhaseNet is a deep learning model developed by W. Zhu & Beroza (2018).

2.3 Results

We compare our seismic event catalog against that from Schoenball et al. (2020) for the stimulations in May 2018, June 2018, July 2018 and December 2018 in Figures 3 and 4. As shown in Figure 3a and 3b, the transfer learning derived seismic events contain similar features as the original catalog. More seismic events were detected from the continuous data using our workflow than the existing techniques. Especially the transfer learned model detected additional events located in the dashed ellipse that formed a clear linear pattern. Comparing Figure 3c and 3d, we also found similar patterns between the initial and the update catalog. Additional seismic events (see events in the dashed ellipse in Figure 3d for an example) were detected for the June 2018 stimulations as well. For the July 2018 stimulations, more seismic events were found by the transfer learned model compared to the initial catalog (Figure 4b). In Figure 4d, we noted a planar feature (in solid ellipse) in both the initial and the updated catalog. The planar feature is tighter in the update catalog than in the initial catalog. A lot more seismic events were identified by the transfer learned model. The distribution of these seismic events shows some compact clusters, which may be related to local fractures that were not detected in the original catalog. Interestingly, a few clusters were active during the May 2018, June 2018 and December 2018 stimulations but not during the July 2018 stimulations.

3. OKLAHOMA REGION

The current state of practice for body wave tomography uses manually measured seismic signal arrival times (or phase picks) as data constraints. Manual picking is the most reliable approach to measure the signal arrival times. Picking these arrival times is very labor-intensive. We have downloaded around 235,000 three-component body wave seismograms for the Oklahoma region. The manual picking step would take a human analyst nearly 6 months to complete. We used a deep learning model (PhaseNet, W. Zhu & Beroza, 2018) to automate and speed up the phase picking step while maintaining human performance. The resulting phase picks were used to image the subsurface structure and improve seismic event locations. Earthquake locations processed by the United States Geological Survey (USGS) are used as the baseline and compared against our results. We used manual phase picks processed by the USGS to improve the seismic event locations and used deep-learning derived phase picks to update the seismic catalog independently. The seismic event locations improved with both manual and deep-learning derived phase picks were compared with the baseline. For seismic events associated with several earthquake sequences, better locations are shown as a tighter linear trend along the faults. Fast and high-precision seismic event catalogs provide us with crucial information for fault detection, site selection and evaluation, background seismicity investigation, and near real-time monitoring.

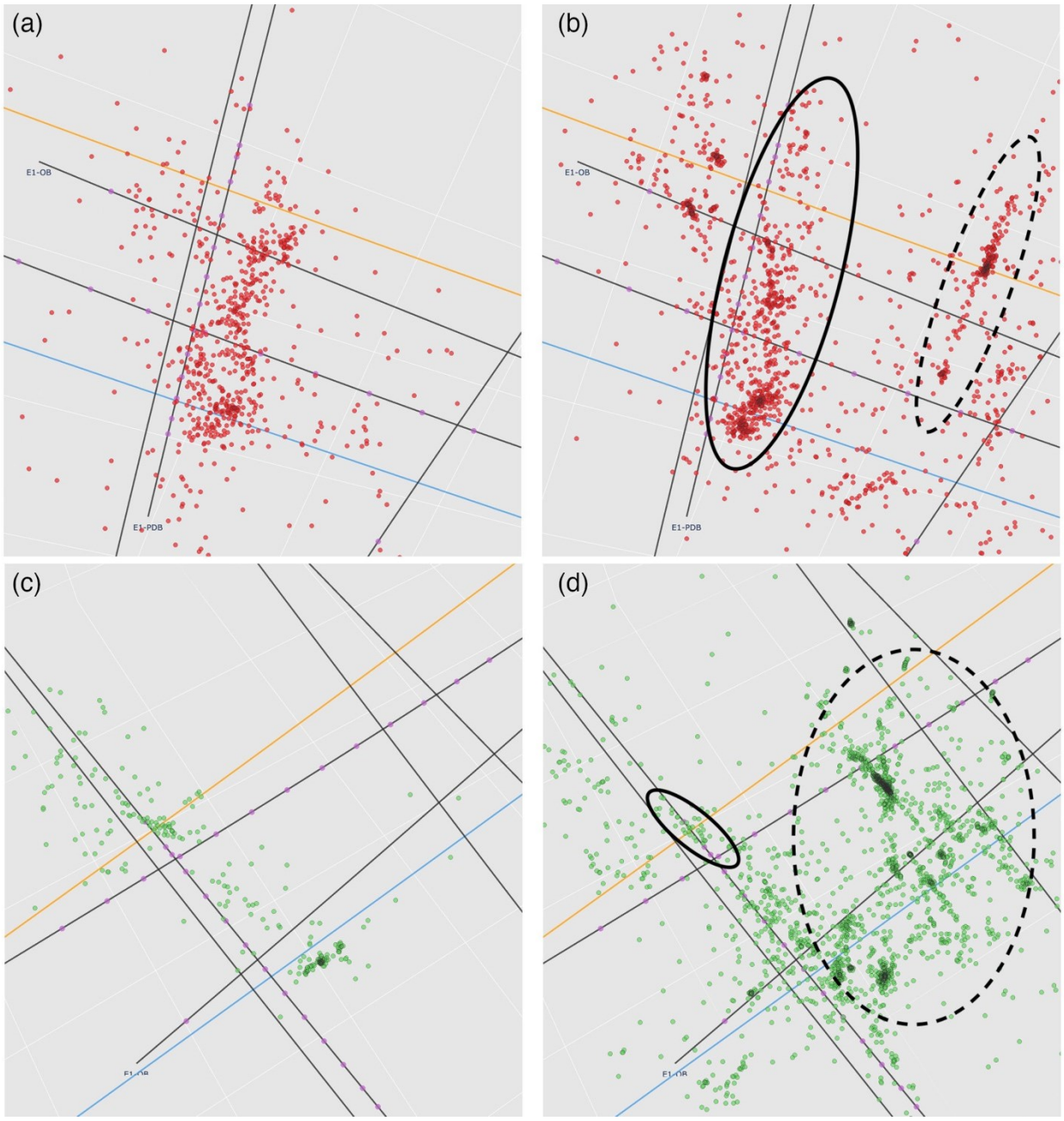

Figure 3: Comparison of the original (a and c) and the updated (b and d) microseismic event locations (dots) associated with the stimulations in May 2018 (a and b) and June 2018 (c and d). The original seismic event locations were obtained from (Schoenball et al., 2020). Seismic events in the right panels (b and d) were updated with transfer-learning picks derived from continuous seismic data. The lines represent boreholes. The solid ellipse indicates similar patterns between the original and the updated seismic event locations. The dashed ellipse shows additional seismic events detected by the transfer learned model from the continuous data.

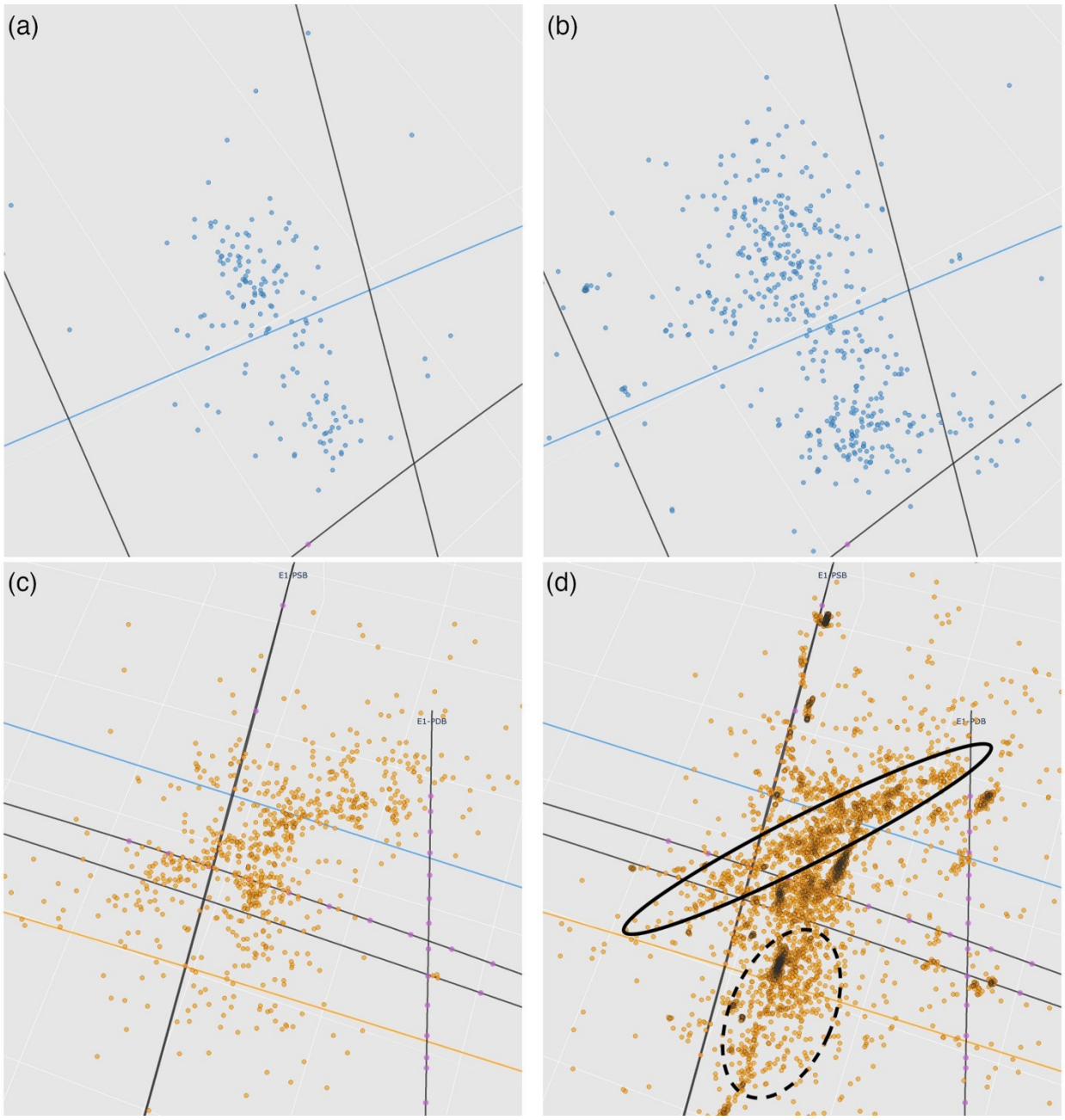

Figure 4: Comparison of the original (a and c) and the updated (b and d) microseismic event locations (dots) associated with the stimulations in July 2018 (a and b) and December 2018 (c and d). The original seismic event locations were obtained from (Schoenball et al., 2020). Seismic events in the right panels (b and d) were updated with transfer-learning picks derived from continuous seismic data. The lines represent boreholes. The dashed ellipse shows additional seismic events detected by the transfer learned model from the continuous data.

3.1 Data

Our data for the Oklahoma region included around 235,000 three-component body wave seismograms downloaded from the Data Management Center of Incorporated Research Institutions for Seismology and associated seismic catalog from USGS. All earthquakes (around 10,700) with recorded manual phase picks from the USGS between 2006 and 2020 were used. A total of 342 seismic stations were used (Figure 1b).

3.2 Method

Our technique integrates deep learning techniques with mature subsurface imaging algorithms (Figure 2). We used the double-difference tomography algorithm (Zhang & Thurber, 2003, 2006) for subsurface imaging and seismic catalog improvement. The double-difference tomography algorithm takes seismic phase picks, an original seismic event catalog, and an initial seismic velocity model as inputs and

produces an updated seismic event catalog and images of the subsurface. The USGS seismic event locations are used as the original seismic event catalog and a baseline. To better validate the improvements of deep learning techniques, we performed double-difference tomography using both manual phase picks and deep-learning derived phase picks. The manual phase picks were obtained from the USGS earthquake catalog. We used the seismic velocity model from Chai, Delorey, et al. (2021) as the initial model. We downloaded three-component seismograms that have manual picks and measured phase picks from the seismograms using a pre-trained deep learning model, PhaseNet (W. Zhu & Beroza, 2018). The manual picking step would take a human analyst nearly 6 months to complete. PhaseNet automates and speeds up the phase picking step while maintaining human performance. The resulting phase picks were used to image the subsurface structure and improve seismic event locations with a double-difference tomography algorithm (Zhang & Thurber, 2003, 2006). We run the tomography algorithm many times using different inversion parameters and identified the optimal set of inversion parameters for both manual and deep-learning picks. The resulting seismic event catalogs derived from both manual and deep-learning picks were compared to the baseline.

3.3 Results

Using body-wave seismograms from the Oklahoma region, we have shown that the deep learning model can significantly speed up the phase picking task. As shown in Table 1, it only takes the deep learning model 38 min on a laptop computer to process all the body-wave seismograms (around 235,000) for the Oklahoma region. However, it would take a human analyst 118 workdays to complete the same task, based on our estimate. Therefore, the deep learning model reduced the processing time by 99.9%. Furthermore, we can easily improve the processing speed of the deep learning model by using more computing resources.

Table 1: Time cost comparison between a human analyst and the deep learning model for body wave phase picking using data from the Oklahoma region.

Approach	Time
Human analyst	118 workdays
Deep learning model	38 mins

Deep learning not only speeds up the phase picking task but also leads to better seismic event locations. As shown in Figures 5 and 6, the double-difference tomography improves the seismic event locations for both manual picks and deep learning derived picks. Since the original event locations are mostly computed assuming 1D layered models, the updated seismic event locations show improvements compared to the USGS catalog by accounting for the 3D heterogeneities in subsurface structure. When we compare event locations updated with deep learning derived picks and manual picks, we noticed tighter linear trends for the deep learning picks. The tighter linear trends provide better constraints on the geometry of fault structures. We also compared the updated seismic event locations against the moment tensor solutions from the Saint Louis University earthquake catalog. The linear trends in our seismic event catalog generally match the fault plane azimuth estimates from the moment tensor solutions (Figures 5 and 6).

We visualized the original and updated seismic event locations with three-dimensional interactive tools (see Figure 7 for screenshots of the tools). Clearly, the seismic event locations derived from manual picks through the double-difference tomography show tighter patterns than the original locations from USGS. The updated seismic catalog using deep learning picks exhibits even tighter patterns than that using manual picks, especially in the vertical direction. The detailed geometry of fault planes is more clearly revealed with the deep-learning derived catalog than the manual picks derived catalog and the USGS catalog. We found multiple fault segments from the deep-learning derived catalog that are not well illustrated with the manual catalog and the USGS catalog. As an example, we fitted two planes (red and blue) for the Mw 5.1 2016 Waynoka earthquake sequence (Figure 8). The blue plane is difficult to constrain with the manual picks derived catalog but is reasonably well constrained in the deep learning derived catalog. With the high-precision catalog obtained with deep-learning picks, we can also study the temporal evolution of the aftershocks. As shown in Figure 9, the rupture initiated on the red plane and propagated to the southwest direction gradually. After around one year, the blue plane ruptured, which has a smaller length than the red plane.

4. DISCUSSION AND CONCLUSIONS

We developed an AI-enhanced seismic monitoring workflow for geothermal and carbon storage purposes. The workflow is applicable to various spatial scales. We have successfully applied it for studies areas at 10-m and 100-km scales. The results for the EGS Collab Experiment 1 show the workflow can process continuous seismic data and produce a high-quality seismic catalog quickly. The resulting seismic catalog contains more seismic events than the existing technique. As demonstrated with seismic data from the Oklahoma region, PhaseNet reduced the time cost of phase picking by 99.9% compared to a human analyst. The deep learning derived phase picks were then used to relocate seismic events as well as to image the 3D subsurface structure. Compared to both the USGS catalog and manual picks derived seismic locations, the deep learning picks lead to more precise seismic event locations. The linear trend of several earthquake sequences was better constrained by deep learning pick derived event locations. The earthquake depth is better constrained with the deep learning picks than the manual picks. With the high-precision catalog derived from deep learning picks, we revealed the detailed geometry of fault planes of the 2016 Waynoka earthquake sequence. The deep learning derived catalog allows us to constrain a secondary fault segment that is not obvious in the USGS catalog and the manual picks derived catalog. The AI-enhance seismic catalog can be used to better study subsurface fault/fracture systems, image the subsurface, and investigate background seismicity.

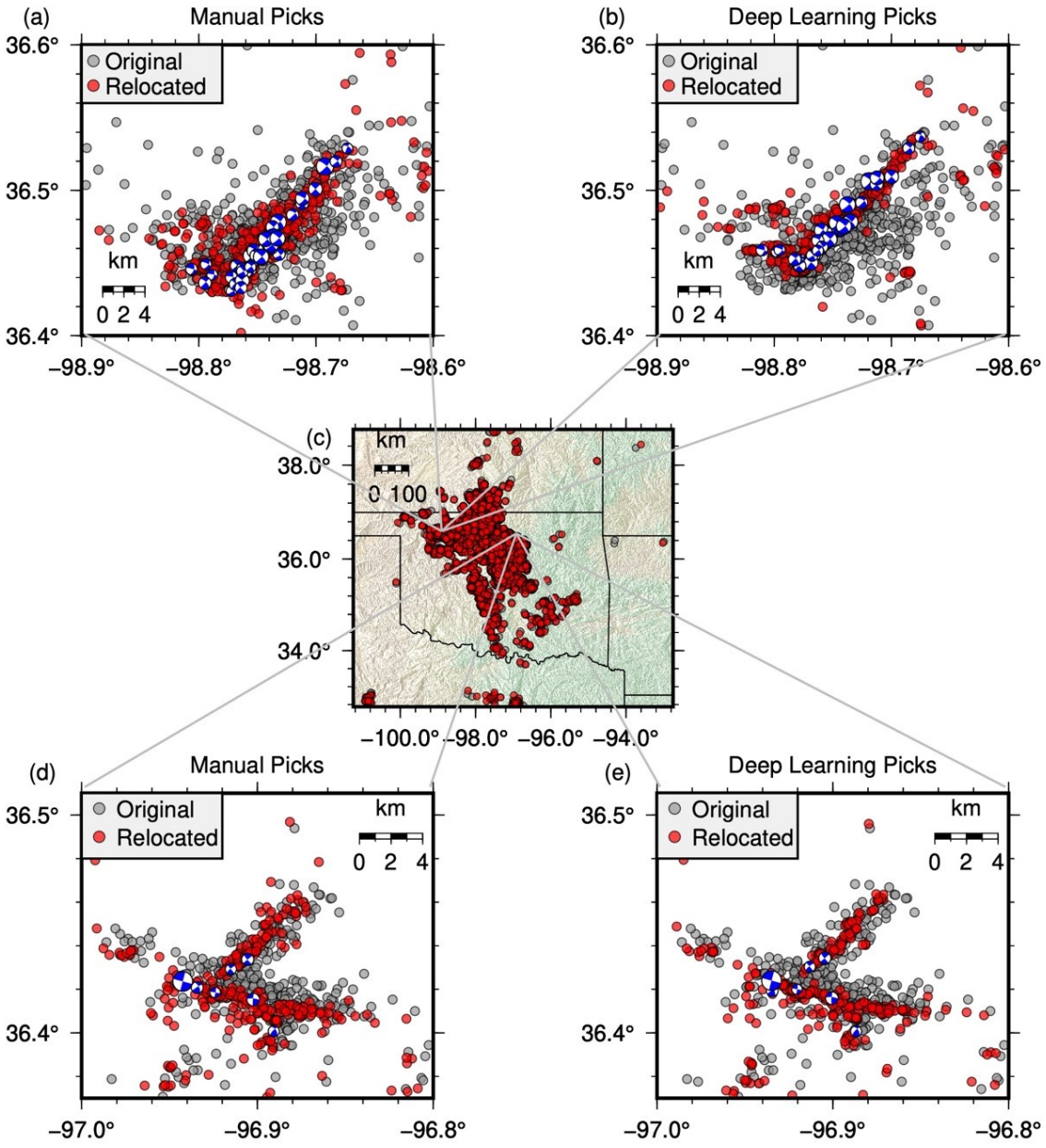

Figure 5: Comparison of the original seismic event locations (gray circles, from USGS), the event locations updated with manual phase picks (red circles and beachballs in panels a and d), and the event locations updated with deep learning picks (red circles and beachballs panels b and e). The locations of panels a, b, d, and e are shown in panel c with the gray lines. Beachballs show earthquake focal mechanisms from the Saint Louis University moment tensor catalog. Panels a and b correspond to the 2016 Waynoka earthquake (Mw 5.1) sequence. Panels d and e show aftershocks of the 2016 Pawnee earthquake (Mw 5.8) sequence.

Our workflow can be used for both surface sensors (Oklahoma region) and borehole monitoring arrays (EGS Collab Experiment 1). We have demonstrated the workflow with the transfer learning technique for borehole sensors (Chai et al., 2020). The workflow can be used before injection to investigate background seismicity and subsurface structure, and after injection for real-time seismic monitoring. We envision daily use of an advanced passive seismic workflow. Using continuous passive seismic data as input, our workflow produces near real-time information about microseismic events. Body-wave arrival times can be combined with other types of observations such as surface-wave dispersion in joint inversion algorithms (e.g., Chai et al., 2019, 2021; Syracuse et al., 2016) to produce 3D elastic property models efficiently and reliably. The elastic properties together with other data constraints can be incorporated for 3D stress modeling (e.g., Chai et al., 2021). AI models and physics-based algorithms can be systematically integrated for near real-time monitoring. The data products from our workflow can provide crucial information for the decision-making of geothermal and carbon storage sites.

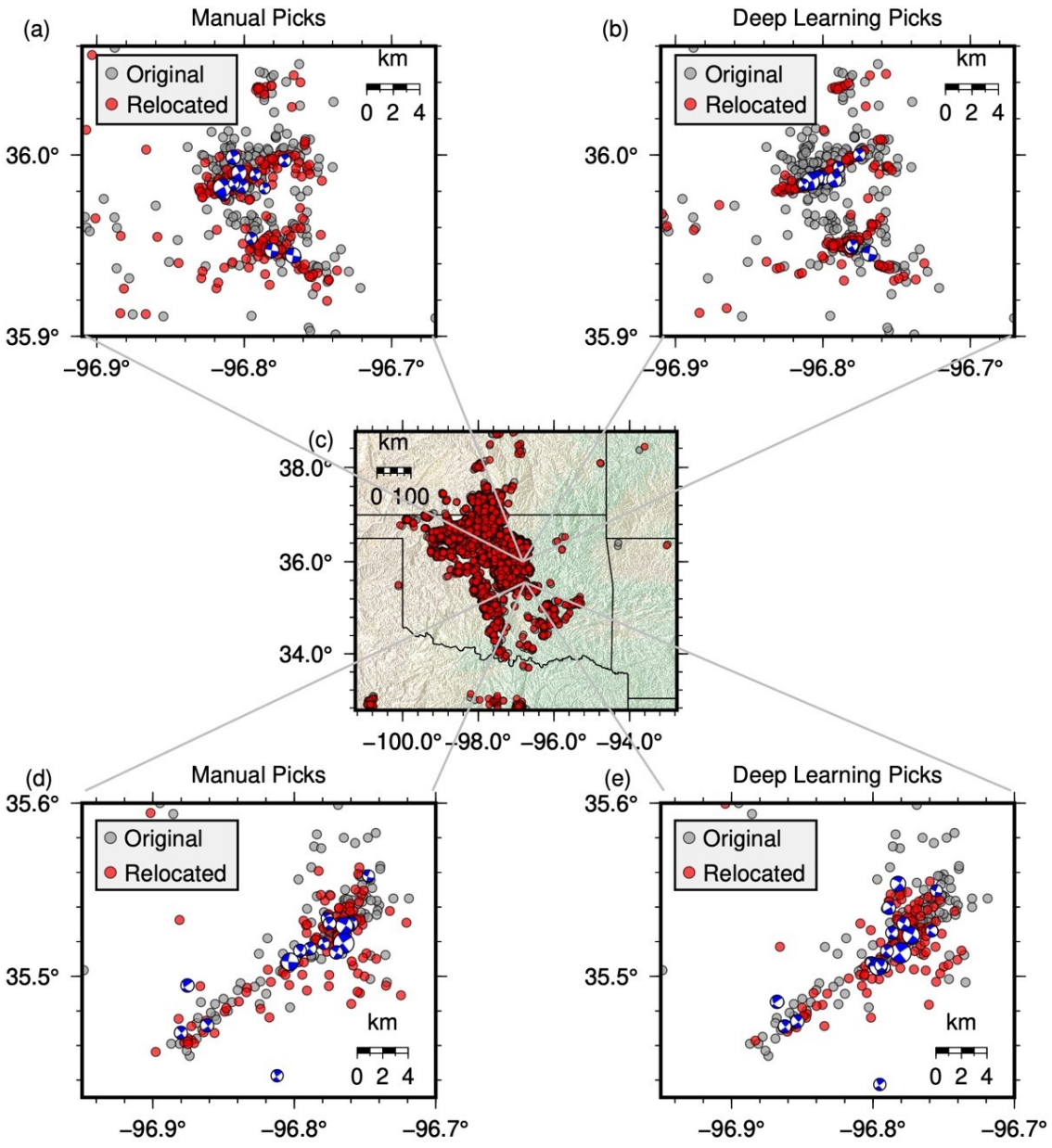

Figure 6: Same as Figure 5 but for the 2016 Cushing (Mw 5.0) earthquake sequence (a and b) and the 2011 Prague earthquake (Mw 5.7) sequence (d and e).

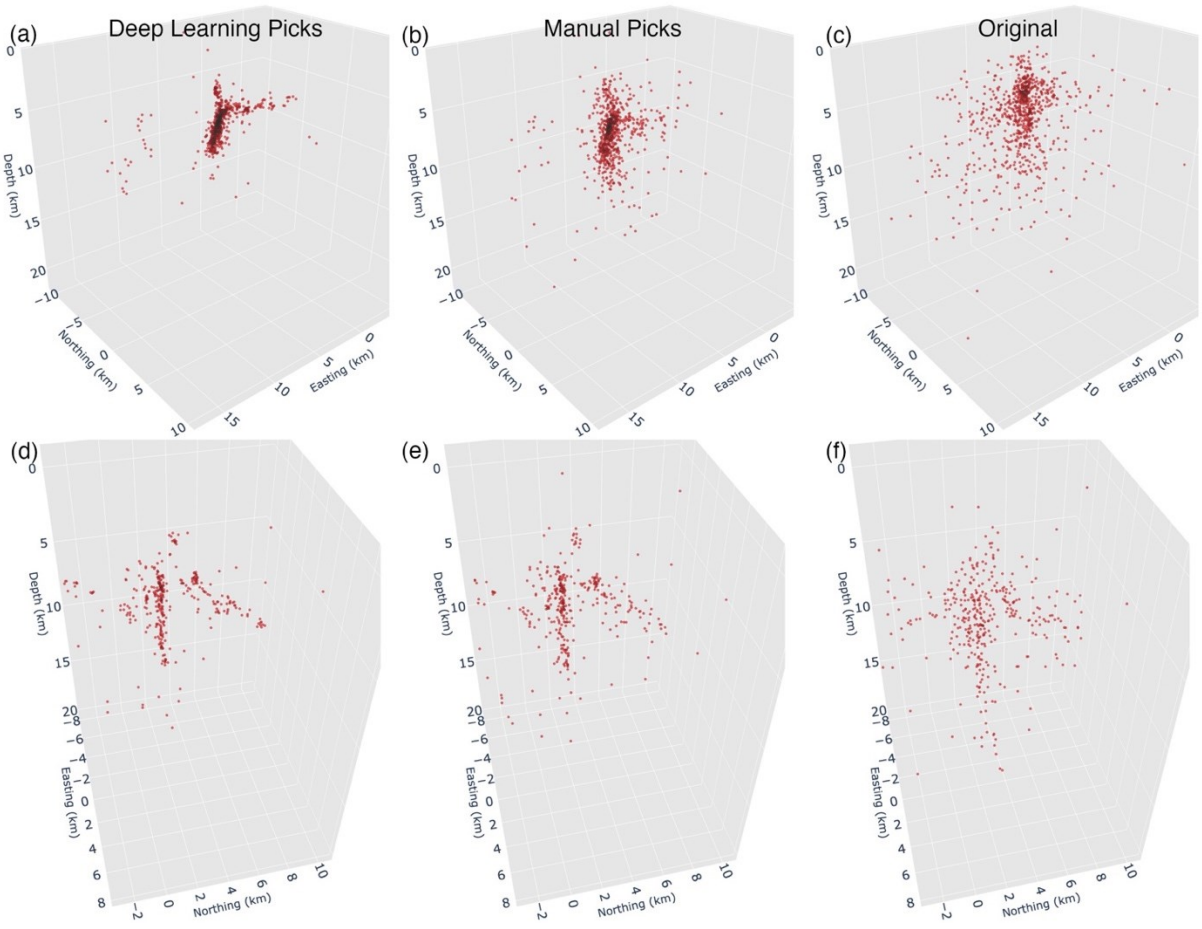

Figure 7: 3D views of seismic event locations for the 2016 Waynoka earthquake sequences (a, b, and c) and the 2016 Pawnee earthquake sequence (d, e, f). Panels a and d show locations updated with deep learning picks. Panels b and e show locations updated with manual picks. Panels c and f are the original locations from USGS.

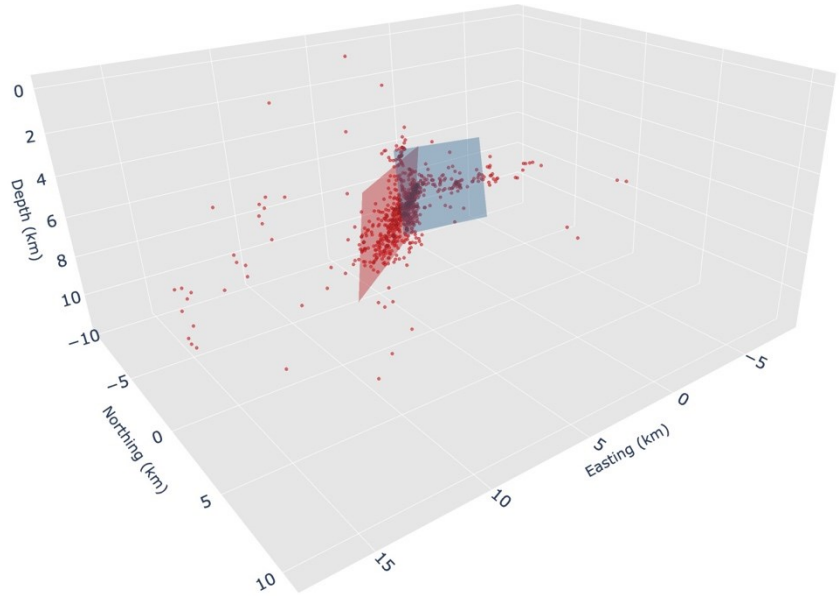

Figure 8: Fitted fault planes using the seismic catalog updated with deep-learning picks for the 2016 Waynoka earthquake sequence.

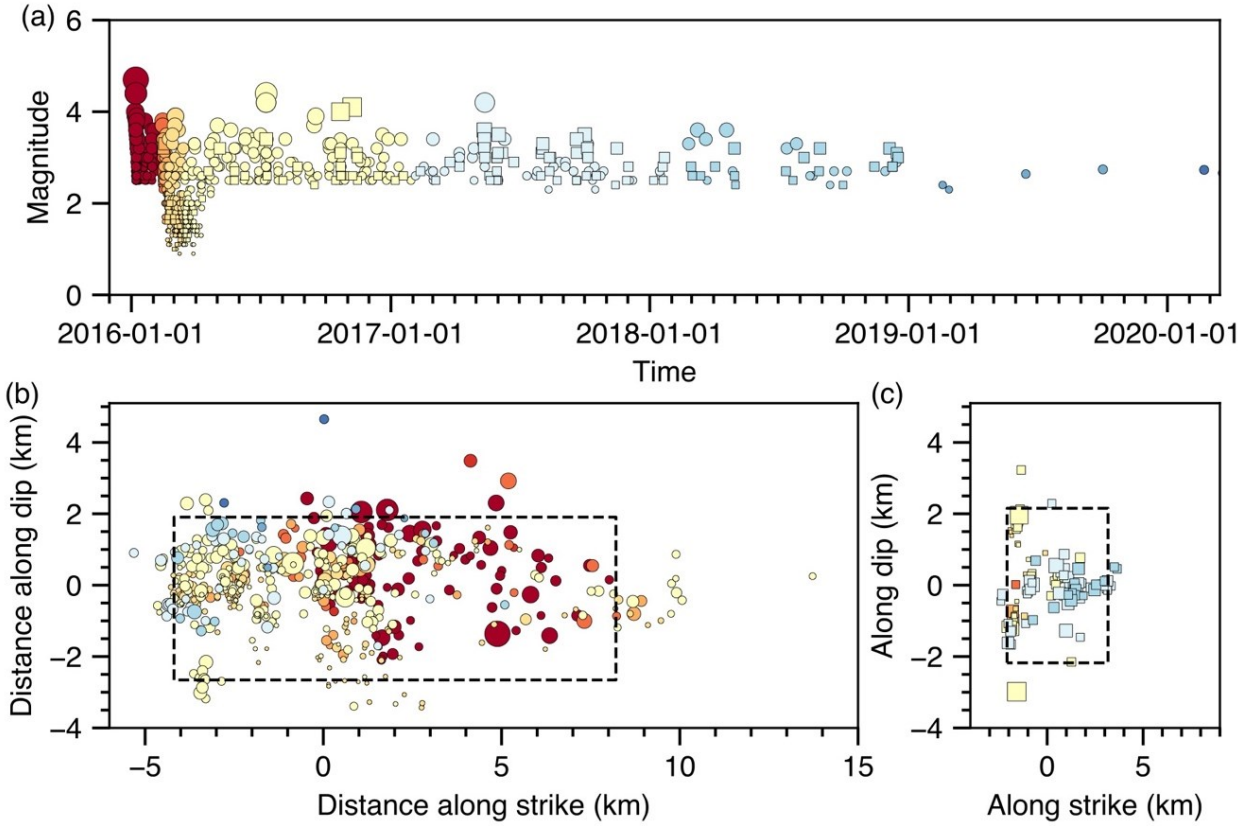

Figure 9: Temporal evolution of the seismic events for the 2016 Waynoka earthquake sequence. The dashed box in panel b indicates the red plane in Figure 8. The dashed box in panel c represents the blue plane in Figure 8. The size and color of symbols in panels b and c are the same as those in panel a. Circles are used for seismic events close to the red plane, while squares are used for seismic events close to the blue plane.

ACKNOWLEDGEMENTS

Portions of this work were supported by the U.S. Department of Energy (DOE), Office of Fossil Energy, Carbon Storage Program through the Science-informed Machine Learning for Accelerating Real-Time Decisions in Subsurface Applications (SMART) Initiative. This material was based upon work supported by the U.S. Department of Energy, Office of Energy Efficiency and Renewable Energy (EERE), Office of Technology Development, Geothermal Technologies Office, under Award Number DE-AC05-00OR22725. The United States Government retains, and the publisher, by accepting the article for publication, acknowledges that the United States Government retains a non-exclusive, paid-up, irrevocable, world-wide license to publish or reproduce the published form of this manuscript, or allow others to do so, for United States Government purposes. The research supporting this work took place in whole or in part at the Sanford Underground Research Facility in Lead, South Dakota. The assistance of the Sanford Underground Research Facility and its personnel in providing physical access and general logistical and technical support is acknowledged. We thank Haijiang Zhang for sharing the tomoDD package. The views and conclusions contained in this document are those of the authors and should not be interpreted as necessarily representing the official policies, either expressed or implied, of the U.S. Government.

REFERENCES

Allen, R. V. (1978). Automatic earthquake recognition and timing from single traces. *Bulletin of the Seismological Society of America*, *68*(5), 1521–1532.

Chai, C., Ammon, C. J., Maceira, M., & Herrmann, R. B. (2018). Interactive Visualization of Complex Seismic Data and Models Using Bokeh. *Seismological Research Letters*, *89*(2A), 668–676. https://doi.org/10.1785/0220170132

Chai, C., Maceira, M., Santos-Villalobos, H., & Team, E. C. (2019). Subsurface Seismic Structure Around the Sanford Underground Research Facility. In *44th Workshop on Geothermal Reservoir Engineering* (pp. 1364–1376). Retrieved from https://www.osti.gov/servlets/purl/1495944

Chai, C., Maceira, M., Santos-Villalobos, H. J., Venkatakrishnan, S. V., Schoenball, M., Zhu, W., et al. (2020). Using a Deep Neural Network and Transfer Learning to Bridge Scales for Seismic Phase Picking. *Geophysical Research Letters*, *47*(16), e2020GL088651. https://doi.org/10.1029/2020GL088651

Chai, C., Delorey, A. A., Maceira, M., Levandowski, W., Guyer, R. A., Zhang, H., et al. (2021). A 3D Full Stress Tensor Model for Oklahoma. *Journal of Geophysical Research: Solid Earth*, *126*(4), e2020JB021113. https://doi.org/10.1029/2020JB021113

Chai, C., Maceira, M., Santos-villalobos, H. J., Singanallur, V., Schoenball, M., Fu, P., et al. (2021). Revealing Fracture Planes with a High-Resolution Catalog of Induced Microearthquakes. https://doi.org/10.1002/essoar.10507602.1

Fu, P., Schoenball, M., Ajo-Franklin, J. B., Chai, C., Maceira, M., Morris, J. P., et al. (2021). Close Observation of Hydraulic Fracturing at EGS Collab Experiment 1: Fracture Trajectory, Microseismic Interpretations, and the Role of Natural Fractures. *Journal of Geophysical Research: Solid Earth*, *126*(7), e2020JB020840. https://doi.org/10.1029/2020JB020840

Klein, F. W. (2002). User's Guide to HYPOINVERSE-2000, a Fortran Program to Solve for Earthquake Locations and Magnitudes. *U.S. Geol. Surv. Open File Report 02-171*. https://doi.org/http://geopubs.wr.usgs.gov/open-file/of02-171/

Mousavi, S. M., Ellsworth, W. L., Zhu, W., Chuang, L. Y., & Beroza, G. C. (2020). Earthquake transformer—an attentive deep-learning model for simultaneous earthquake detection and phase picking. *Nature Communications*, *11*(1), 3952. https://doi.org/10.1038/s41467-020-17591-w

Ross, Z. E., Meier, M.-A., & Hauksson, E. (2018). P Wave Arrival Picking and First-Motion Polarity Determination With Deep Learning. *Journal of Geophysical Research: Solid Earth*, *123*(6), 5120–5129. https://doi.org/10.1029/2017JB015251

Schoenball, M., Ajo-Franklin, J. B., Blankenship, D., Chai, C., Chakravarty, A., Dobson, P., et al. (2020). Creation of a Mixed-Mode Fracture Network at Mesoscale Through Hydraulic Fracturing and Shear Stimulation. *Journal of Geophysical Research: Solid Earth*, *125*(12), 1–21. https://doi.org/10.1029/2020JB019807

Syracuse, E. M., Maceira, M., Prieto, G. A., Zhang, H., & Ammon, C. J. (2016). Multiple plates subducting beneath Colombia, as illuminated by seismicity and velocity from the joint inversion of seismic and gravity data. *Earth and Planetary Science Letters*, *444*, 139–149. https://doi.org/10.1016/j.epsl.2016.03.050

Zhang, H., & Thurber, C. (2003). Double-difference tomography: the method and its application to the Hayward Fault, California. *Bulletin of the Seismological Society of America*, *93*(5), 1875–1889. https://doi.org/10.1785/0120020190

Zhang, H., & Thurber, C. (2006). Development and Applications of Double-difference Seismic Tomography. *Pure and Applied Geophysics*, *163*(2–3), 373–403. https://doi.org/10.1007/s00024-005-0021-y

Zhou, Y., Yue, H., Zhou, S., & Kong, Q. (2019). Hybrid event detection and phase-picking algorithm using convolutional and recurrent neural networks. *Seismological Research Letters*, *90*(3), 1079–1087. https://doi.org/10.1785/0220180319

Zhu, L., Peng, Z., McClellan, J., Li, C., Yao, D., Li, Z., & Fang, L. (2019). Deep learning for seismic phase detection and picking in the aftershock zone of 2008 M7.9 Wenchuan Earthquake. *Physics of the Earth and Planetary Interiors*, *293*(May 2018), 106261. https://doi.org/10.1016/j.pepi.2019.05.004

Zhu, W., & Beroza, G. C. (2018). PhaseNet: A Deep-Neural-Network-Based Seismic Arrival Time Picking Method. *Geophysical Journal International*, *216*(1), 261–273. https://doi.org/10.1093/gji/ggy423